Hindawi
Journal of Chemistry
Volume 2022, Article ID 8448260, 20 pages
https://doi.org/10.1155/2022/8448260

Research Article

An Approach for Modeling, Simulation, and Optimization of Catalytic Production of Methyl Ethyl Ketone

Zahra Parhizi,[1] **Milad Nayebi**,[1] **Edris Mohammadzadeh**,[2] **and Reza Torfi**[3]

[1]*Chemical Engineering Department, Amirkabir University of Technology, Tehran, Iran*
[2]*Department of Chemical Engineering, Faculty of Engineering, Kermanshah University of Technology, Kermanshah, Iran*
[3]*School of Chemical, Petroleum and Gas Engineering, Iran University of Science & Technology, Tehran, Iran*

Correspondence should be addressed to Zahra Parhizi; zariparhizi@gmail.com

Received 15 April 2022; Revised 10 September 2022; Accepted 15 September 2022; Published 13 October 2022

Academic Editor: S. Shanmuga Priya

The current exploration manifests the progress of a one-dimensional reactor for the production of methyl ethyl ketone (MEK) as a commercial-industrial solvent with a relatively rapid evaporation rate and high solvation ability. MEK has been extensively utilized in colorings, printing, artificial leather, and base oils. One of the methods for the production of MEK is catalytic dehydrogenation of 2-butyl alcohol in the temperature range of 650–750 K utilizing spherical ZnO catalyst. Considering the high cost of fossil fuels to achieve optimal energy consumption, thermal coupling with the Fischer–Tropsch reaction was employed. Eventually, an evolutionary genetic algorithm was adopted to optimize the reactor to maximize MEK production. MATLAB software was utilized for the modeling and optimization. The modeling results were verified by industrial data. Moreover, they indicated a 37 and 55.4% increase in the production rate of thermal coupling and optimal thermal coupling reactors, respectively.

1. Introduction

Considering the ongoing depletion of fossil fuel resources and the escalation of global warming, hydrogen seems to be the future energy carrier. Hydrogen has been considered as an alternative renewable carrier of energy. Regarding the day-by-day increase in hydrogen demand, various methods have been developed to increase hydrogen production. Catalytic modification of natural gas and other hydrocarbons is one of the major routes for hydrogen production. The use of this method will result in the emission of greenhouse gases (GHGs) as well as corrosive ones such as CO_2 and CO. One of the approaches for the storage and transfer of hydrogen is the dehydrogenation of high-content organic hydrocarbons. One of the objectives of this study is to simulate a two-reaction thermal coupling reactor for simultaneous production of hydrogen and methyl ethyl ketone (MEK) utilizing the concept of process intensification (PI). Since 1970, PI has been utilized as a new approach in the design of chemical engineering processes, reactors have been regarded as the core-foundation-pillars of the chemical industry [1, 2]. Reactors can reduce process costs and energy consumption. Fischer–Tropsch (FT) process is highly exothermic and comprises a series of exothermic reactions. Thermal coupling of this reaction can reduce the cost of cooling processes and the reaction heat can be utilized in the endothermic reaction of MEK production. This method relies on increasing the simultaneous production of energy and substances. Innovations in catalytic reactor technology are often preferred as the starting point of this trend. In this regard, the thermal multipurpose reactor is a new concept in PI. Thermal coupling of endothermic and exothermic reactions is a branch of multipurpose reactors. In this type of reactor, an exothermic reaction is considered as a heat source of an endothermic reaction. Recently, extensive investigations have been devoted to the catalytic dehydrogenation reaction of 2-butanol and MEK production [3–5]. The coupling of endothermic and exothermic reactions has been identified as an effective method to progress the performance of processes. In particular, the literature is replete with excellent examples of thermally coupled reactors [6–8]. Accordingly, the conventional

Table 1: Comparison of review articles.

Authors	Year	Subject
Keuler et al. [9]	2002	Dehydrogenation of 2-butanol in Pd-Ag membrane reactor
Lightard et al. [10]	2002	Sustainable catalyzed dehydrogenation of alcohols by hydrogen gas circulation
Liu et al [11]	2006	Investigation of synthesis technology and catalyzed hydration of butylene for MEK production
Fang et al. [12]	2009	Using a new mesoporous catalyst (Cu-Zn-Al_2O_3), they investigated the dehydrogenation of alcohol
Multer et al. [13]	2012	Production of MEK by a hybrid biochemical method using biomass
Dehkordi at al. [14]	2022	Degradation of dissolved RDX, NQ, and DNAN by cathodic processes in an electrochemical flow-through reactor.
Katoch et al. [15]	2021	A review on genetic algorithm: past, present, and future.
Marvast et al. [16]	2005	Fischer–Tropsch synthesis: modeling and performance study for Fe-HZSM5 bifunctional catalyst.
Ebrahimi et al. [17]	2022	Crosstalk between ferroptosis and the epithelial-mesenchymal transition: implications for inflammation and cancer therapy.

reactors in the MEK production have been replaced with the new multifunctional reactors. In pursuit of these, the current study aims to integrate the MEK production and 2-butanol dehydrogenation process in a novel thermally coupled reactor concept in which the required heat for the dehydrogenation reaction is supplied by the FT reaction by gas to liquid (GTL) method as an exothermic reaction. Remarkably, this concept leads to a significant decrease in operational costs and energy consumption due to the elimination of certain equipment. It is worthy to note that the mentioned coupled reactor decreases the size of the reactor. Moreover, the thermal coupling can increase the reaction rate as well as the reactor equilibrium conversion. Interestingly, simultaneous production of different products as well as preventing the formation of unwanted products can be considered as another benefit of the current reactor. Finally, an evolutionary genetic algorithm was used to optimize the reactor for maximizing MEK production. In the second section, the previous works in the field of production and modeling of MEK and dehydrogenation of 2-butanol are discussed. The modeling and numerical methods are stated in the third section; while the evaluation and its results are presented in the fourth section.

2. Literature Review

Numerous studies have addressed the production and modeling of MEK production as well as 2-butanol dehydrogenation which are summarized in Table 1. In [9], the dehydrogenation of 2-butanol to methyl ethyl ketone (MEK) was explored in a membrane reactor including Pd-Ag film (2.2 m thickness) deposited on the inside of an α-alumina tube and packed with a 14.4 wt.% Cu on SiO_2 catalyst. Conducting experiments at temperatures of 190 to 240°C specifies a better performance of the membrane reactor of 2-butanol conversions than the plug flow reactor. Significantly, the 2-butanol conversion increased with an augmentation in the sweep gas flow rate, but reduced with an upsurge in the 2-butanol feed flow rate. It is worthy to note that in all the tests performed, the selectivity for MEK production was above 96%.

Fatholahi et al. in [10] manifests the catalytic dehydrogenation of alcohols into aldehydes and ketones in the presence of transition metal catalysts like $Ru(OCOCF_3)_2(CO)(PPh_3)_2$. One of the advantages of using Robinson's catalyst is the conversion of secondary alcohol to the corresponding ketones with high selectivity in relatively short reaction times. Moreover, the catalyst could be recovered three times without main loss in catalytic activity.

Another methodology for the synthesis of methyl ethyl ketone (MEK) is designed and suggested in [11]. Accordingly, secondary butanol (SBA) is produced from catalytic hydration of butylene. Subsequently, MEK synthesis was carried out by dehydrogenation of SBA. Successfully, the designed and optimized methodology has also shown highly promising results with high catalyst activity, good selectivity, and long lifespan.

In [12], a series of meso-structured Cu-Zn-Al_2O_3 has been synthesized and characterized using XRD, N_2 physical adsorption, and TPR procedures. In the next step, their catalytic activity was investigated for dehydrogenation of 2-butanol to methyl ethyl ketone (MEK) at atmospheric pressure. Interestingly, the results corroborated that the mesoporous Cu-Zn-Al_2O_3 catalysts were promising in the production of MEK and disapproving for the formation of by-products than the catalysts synthesized by coprecipitation technique.

Research in the area of biomass conversion to fuels and chemicals has recently gained much importance in sustaining the progress of biochemical and chemical processes. In [13], production of MEK by a hybrid biochemical method using biomass was explored. In this circumstance, 2,3-butanediol was synthesized through the microbial fermentation (the bacteria *Klebsiella* oxytoca (K.O) was used). In the second step, using dehydration over a solid acid catalyst, MEK was produced from the conversion of 2,3-butanediol. It is worth noting that dehydration kinetics were dependent on the concentration of 2,3-butanediol with a slightly higher reaction order than one (1.22).

3. Modeling Approaches

MEK is currently produced on commercial scales using a two-stage N-butylene method involving hydration of butylene to produce 2-butyl alcohol (SBA) followed by dehydrogenation SBA and production of MEK. Depending on the catalyst, there exist three main steps: indirect hydration of sulfate, direct hydration of resin, and direct hydration of

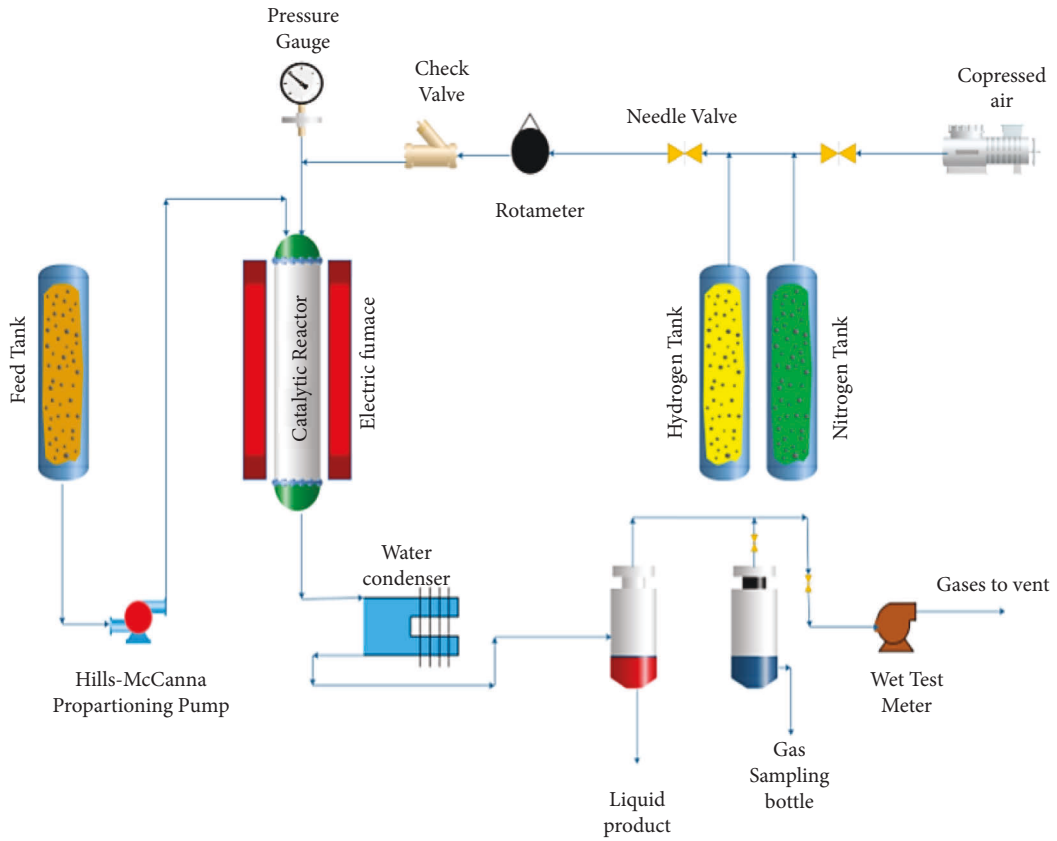

Figure 1: Diagram of the equipment for dehydrogenation of 2-butyl alcohol [18–20].

acid. This method is benefited from high MEK selectivity (about 95%), facile separation of product and dehydrogenation of the vapor phase, high 2-butanol conversion, and lower energy consumption. This process has low economic advantages relative to the dehydrogenation of 2-butanol; the main factor is, however, accessibility and cost of n-butane. Compared to all processes, the dehydrogenation of 2-butanol has higher advantages in addition to its cost-effectiveness. Therefore, this method was selected.

3.1. Kinetics of Dehydrogenation Reaction. As mentioned earlier, this paper addresses the dehydrogenation of 2-butanol (2-butyl alcohol) for MEK production. This reaction is homogeneous and proceeds in the gaseous phase. Hydrogen gas and MEK are the products of this catalytic reaction. The kinetics of this reaction will be discussed in the following equation.

$$r_A = \frac{C\left[p_{Ai} - \left(p_{Ki}p_{Hi}/K\right)\right]}{p_{Ki}\left[1 + K_A p_{Ai} + K_{AK}\left(p_{Ai}/p_{Ki}\right)\right]}. \quad (1)$$

In the above equation, p_{Ai}, p_{Ki}, and p_{Hi} denote the partial pressures of 2-butanol, MEK, and hydrogen on the catalyst surface (in atm), respectively. Moreover, C, K_A, and K_{AK}, respectively, represent the reaction rate constant, the equilibrium constant of 2-butanol adsorption, and the equilibrium adsorption constant of the reaction with the following equations:

$$\log C = \frac{-10735}{T} + 7.776,$$
$$\log K_A = \frac{-6165}{T} + 5.327, \quad (2)$$
$$\log K_{AK} = \frac{486}{T} - 0.1968.$$

K in the above equations refers to the chemical equilibrium constant which was first expressed by Kolb and Burwell as:

$$\log K = \frac{-2790}{T} + 1.510 \log T + 1.865. \quad (3)$$

T is in Kelvin in all the equations.

Figure 1 illustrates a schematic representation of 2-butanol dehydrogenation for the production of MEK.

3.2. Dehydrogenation Reaction. Kinetics of 2-butyl alcohol catalyzed dehydrogenation was examined to produce MEK at atmospheric pressure and various temperatures (650–750 K) in the presence of spherical ZnO catalysts. Thanks to its nature, this catalyst makes it possible to directly evaluate the surface involved in the reaction and define the ratio of surface to the feed (known as S/F) instead of the weight ratio of the feed (W/F) which is common in catalysis studies. The feed composition varied from 2-butyl alcohol to

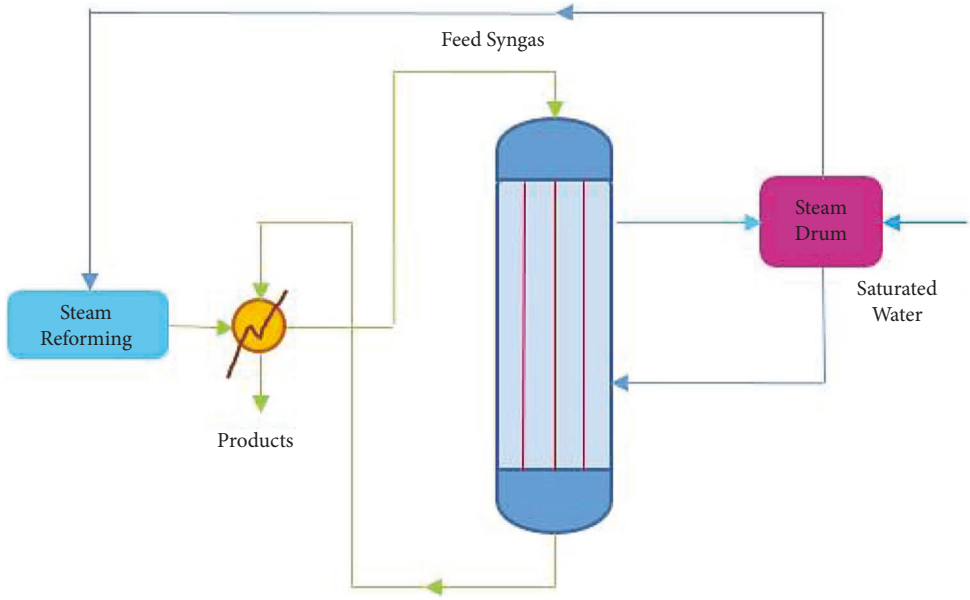

Figure 2: Diagram of F-T reaction process [19].

a mixture with high MEK content. In these studies, the mass transfer effects were considerable and should be considered as an indicator of the catalyst surface condition. Investigation of the effect of feed composition on the initial reaction rate showed that dehydrogenation was the controlling stage which involved a single-site mechanism. Moreover, these results were used to determine the values of the height of the reactor unit (HRU) to relate the mass rate with temperature. HRU provides a simple approach for calculating the depth required to reach a proper conversion percentage [21, 22].

3.3. Kinetics of Fischer–Tropsch Reaction. Compounds such as C_5^+, n-C_4H_{10}, i-C_4H_{10}, C_2H_4, C_2H_6, C_3H_8, CO_2, CO, H_2, H_2O, and CH_4 are involved in the FT reaction. The following reactions occur in the exothermic part of the thermal coupling [23]:

$$\begin{aligned} CO + 3H_2 &\longrightarrow CH_4 + H_2O, \\ 2CO + 4H_2 &\longrightarrow C_2H_4 + 2H_2O, \\ 2CO + 5H_2 &\longrightarrow C_2H_6 + 2H_2O, \\ 3CO + 7H_2 &\longrightarrow C_3H_8 + 3H_2O, \\ 4CO + 9H_2 &\longrightarrow n - C_4H_{10} + 4H_2O, \\ 4CO + 9H_2 &\longrightarrow i - C_4H_{10} + 4H_2O, \\ 6.05CO + 12.23H_2 &\longrightarrow C_{6.05}H_{12.36}\,(C5+) + 6.05H_2O, \\ CO + HH_2O &\leftrightarrow CO_2 + H_2. \end{aligned} \tag{4}$$

During this process which involves gas to liquid conversion, hydrogen and carbon dioxide are mixed in various stoichiometric coefficients to form heavier hydrocarbons [23–25]. Figure 2 schematically illustrates the reaction [19].

3.4. Effective Parameters of the Reaction. The design of the catalytic reactor requires extensive knowledge of the reaction mechanism on the catalyst surface. These mechanisms are different and their development has been reviewed elsewhere [26]. Catalytic reactions occur in the presence of porous catalysts. For this purpose, reactants and products should diffuse each other. Various variables can affect the diffusion into the catalyst pores. For small catalyst sizes, these diffusive effects will not have a drastic impact on the conversion percentage of the reactor substrate [8, 27]. For larger particles on the fixed-substrate reactor, diffusion into or out of the catalyst could be significant, entering an extra variable in the reaction mechanism. By using solid brass metallic particles as catalysts for dehydrogenation of 2-butyl alcohol, in addition to removing this possible variable, it will be possible to directly calculate the involved area. As the area involved in the reaction can be calculated, the relationship between the spatial rate and conversion percentage (dx_A) for the initial part of the reactor with an area of dS can be expressed by [26, 28]:

$$dx_A = r_A \frac{dS}{F}. \tag{5}$$

according to (1), surface-to-feed ratio (S/F), which is directly related to the spatial rate, can be defined as a variable of conversion percentage and reaction rate [26]:

$$\frac{S}{F} = \int_0^x \frac{dx}{r_A}. \tag{6}$$

S/F is simpler and is used instead of W/F. For porous catalysts, W/F depends on the catalyst type, preparation method, and particle size. On the other hand, S/F is more basic as it only depends on the reaction nature and is independent of the S/F ratio [8, 26]. The application of the mechanical stirrer makes it possible to reach higher conversion rates and hence higher temperatures [26]. Since feed rate is not effective in controlling this system, it can be

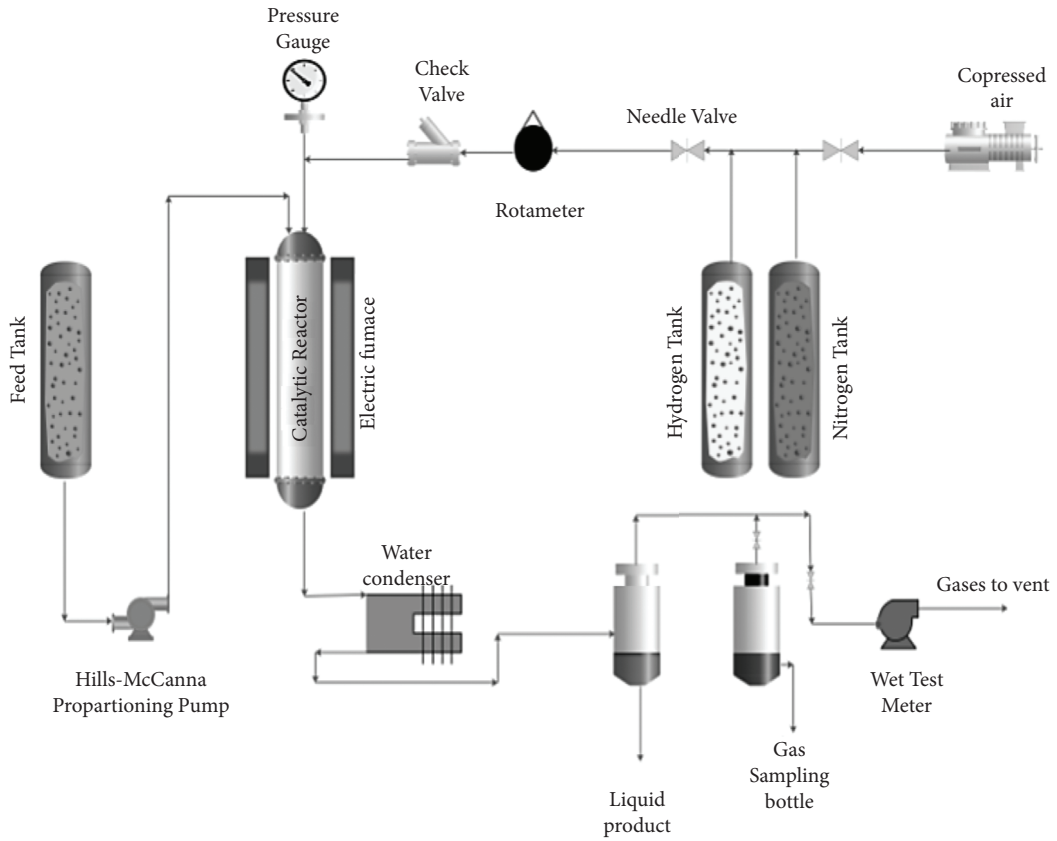

Figure 3: Experimental setup [26].

considered a small value to reach high conversion percentages at lower temperatures. Therefore, more than one temperature may be employed [26]. In an agitated reactor mass, the transport effects can be removed by increasing the flow rate [29].

3.5. Experimental Apparatus. Figure 3 schematically represents the experimental setup of this study. This setup included a small continuous pilot encompassing a stainless steel tube. The reaction feeding was supplied by an electric furnace. The liquid mixture of 2-butyl alcohol and MEK was pumped from a calibrated feed tank [29]. The input hydrogen, nitrogen, and air were also regulated by a needle valve. The flow intensity was measured by a rotameter. To assess the production rate, the reactor effluent was first passed through a condenser and then a phase separator in which the incompressible gases can be collected on the water and salt or passed into the hygrometer [26, 30].

3.6. Selecting the Proper Model to Describe the Reactor. A one-dimensional model in the axial direction is generally used to model MEK production reaction as it is endothermic and the reaction site length is larger than the catalyst tube. Therefore, a one-dimensional steady-state was utilized for the simulation. Furthermore, the mass-energy equilibrium equations will be discussed.

3.6.1. Mass-Energy Balance Equations. To model MEK production, a one-dimensional model in the axial direction is generally used as the reaction is endothermic and the reaction site length is larger than the catalyst tube. Therefore, a one-dimensional steady-state approach was utilized for the simulation. The mass-energy balance equations are as follows:

3.6.2. Mass-Energy Balance Equations. Mass balance:

$$u\frac{\partial c_i}{\partial z} = \frac{\rho_B}{\varepsilon}\sum_{j=1}^{r} v_{i,j} r_j. \tag{7}$$

Energy balance:

$$u\rho_f C_p \frac{\partial T}{\partial z} = \frac{4}{D}U\left(T - T_c\right) + \frac{\rho_B}{\varepsilon}\sum_{j=1}^{r}\left(-H_j\right)r_j. \tag{8}$$

Boundary conditions:

$$\begin{aligned} Z &= 0 c_i = c_{i0}, \\ Z &= 0 T = T_0, \\ Z &= 0 T = T_w. \end{aligned} \tag{9}$$

The following assumptions were considered to model the rector:

(i) The transport mechanism is in the axial direction and in the form of plague

(ii) The pressure drop is negligible along the reactor

(iii) Axial, thermal, and mass scattering were neglected

(iv) The process is steady and one-dimensional;

Equations of FT reaction (exothermic).
Mass balance of the exothermic part:

$$-\frac{1}{A_c}\frac{\mathrm{d}F_i}{\mathrm{d}z}+\sum_{j=1}^{r}\nu_{i,j}\eta_j r_j=0. \tag{10}$$

Energy balance of the exothermic part:

$$u\rho_f C_p\frac{\partial T_{\mathrm{Exo}}}{\partial z}=\sum_{i}^{n} r_i\eta_i\left(-\Delta H_i\right)-\frac{4}{D}U\left(T_{\mathrm{Endo}}-T_{\mathrm{Exo}}\right). \tag{11}$$

Boundary condition of the exothermic part:

$$z=0C=C_{i0\mathrm{Exo}}T=T_{0\mathrm{Exo}}P=P_{0\mathrm{Exo}}. \tag{12}$$

Equation of the dehydrogenation part (endothermic).
Mass balance of the endothermic part:

$$\frac{1}{A_c}\frac{\mathrm{d}F_i}{\mathrm{d}_z}+\sum_{j=1}^{r}\nu_{i,j}r_j=0. \tag{13}$$

Energy balance of the endothermic part:

$$u\rho_f C_p\frac{\partial T_{\mathrm{Endo}}}{\partial z}=\sum_{i}^{n} r_i\eta_i\left(-\Delta H_i\right)-\frac{4}{D}U\left(T_{\mathrm{Exo}}-T_{\mathrm{Endo}}\right). \tag{14}$$

Boundary condition of the endothermic part:

$$z=0\mathrm{C}=C_0T=T_0. \tag{15}$$

3.6.3. Mass and Energy Balance in the Thermal Coupling Condition. Mass balance:

$$u\frac{\partial c_i}{\partial z}=\frac{\rho_B}{\varepsilon}\sum_{j=1}^{r}\nu_{i,j}r_j. \tag{16}$$

Energy balance:

$$u\rho_f C_p\frac{\partial T}{\partial z}=\frac{4}{D}U\left(T_{\mathrm{Exo}}-T_{\mathrm{Endo}}\right)+\frac{\rho_B}{\varepsilon}\sum_{j=1}^{r}\left(-H_j\right)r_j. \tag{17}$$

3.6.4. Mass Balance in the 2-butanol Dehydrogenation.

$$u\frac{\partial c_i}{\partial z}=\sum_{j=1}^{r}\nu_{i,j}r_j. \tag{18}$$

Energy balance in the 2-butanol dehydrogenation:

$$u\rho_f C_p\frac{\partial T_c}{\partial z}=\frac{4}{D}U\left(T-T_c\right)+\sum_{j=1}^{r}\left(-H_j\right)r_j. \tag{19}$$

Boundary condition of both parts:

$$\begin{aligned} z&=0c_i=c_{i0},\\ z&=0T=T_0. \end{aligned} \tag{20}$$

3.7. Auxiliary Equations. In this section, auxiliary equations of the model are presented for the prediction of the physical properties as well as heat transfer.

3.7.1. Heat Transfer Coefficient. The following equation can be employed to determine the total heat transfer between the tubes and reactor shell:

$$U_o=\frac{1}{(1/hi)+(\mathrm{d}i\ln(\mathrm{d}o/\mathrm{d}i)/2k)+\mathrm{d}i/doho}. \tag{21}$$

The heat transfer between the shell and tubes can be neglected due to the thin tubes. The above equation can thus be simplified as:

$$U_o\frac{1}{(1/hi)+(\mathrm{d}i/doho)}. \tag{22}$$

In which the internal heat transfer of the tubes can be determined by:

$$hi=\frac{Nuk_f}{d_p}. \tag{23}$$

In which K_f, d_P, and Nu, respectively, denote the fluid heat transfer coefficient, catalyst diameter, and Nusselt number.

$$Nu+0.015+0.29\mathrm{Re}_d. \tag{24}$$

The Reynolds number can be defined as:

$$\mathrm{Re}_d=\frac{\rho_f u d_p}{u_f}. \tag{25}$$

The density can be determined by:

$$\rho_f=\sum_{i}\frac{P_i Mw_i}{RT}. \tag{26}$$

3.7.2. Heat Capacity. The thermal dependence of the heat capacity of the gases can be expressed by:

$$C_P^o=C1+C2\left[\frac{C3/T}{\sinh(C3/T)}\right]^2+C4\left[\frac{C5/T}{\cosh(C5/T)}\right]^2. \tag{27}$$

3.7.3. Viscosity. Regarding the input feed and reactants, the temperature dependence of the viscosity can be written as:

$$\mu=\frac{C1T^{C2}}{1+(C3/T)+\left(C4/T^2\right)}. \tag{28}$$

3.7.4. Thermal Conduction Coefficient of the Fluid. The temperature dependence of the thermal conduction coefficient can be defined by:

$$k=\frac{C1T^{C2}}{1+(C3/T)+\left(C4/T^2\right)}. \tag{29}$$

3.7.5. Standard Formation Enthalpy. Standard formation enthalpy refers to the amount of enthalpy of a reaction in which one mole of the compound is formed under standard conditions (for pure material; the pressure of 1 atm, $T = 25^{\circ}\mathrm{C}$).

For the following reaction;

$$aA + bB + \ldots \longrightarrow rR + sS + \ldots \tag{30}$$

The formation enthalpy can be defined as:

$$H_f = \left(rH_{fR} + sH_{fS} + \ldots\right) - \left(aH_{fA} + bH_{fB} + \ldots\right). \tag{31}$$

3.8. One-Dimensional Modeling of the Reaction. First, the Peclet number (Pe) is described to clarify the reason for the one-dimensional modeling. Pe is a dimensionless number used in studying the transport phenomena. This number can be defined as the ratio of convective transport flux to diffusive transport flux with the following form:

$$\mathrm{Pe} = \frac{\text{convective transport flux}}{\text{diffusive transport flux}},$$

$$\mathrm{Pe\,(Mass)} = \mathrm{Re} * \mathrm{Sc} = \frac{\rho U D_p}{\mu} * \frac{\mu}{\rho D_{AB}} = \frac{U D_p}{D_{AB}}, \tag{32}$$

$$\mathrm{Pe\,(Heat)} = \mathrm{Re} * \mathrm{Pr} = \frac{\rho U D_p}{\mu} * \frac{\mu C_p}{k} = \frac{\rho U C_p D_p}{k}.$$

As Pe = 10 for the fixed-substrate reactors and Pe of this modeling varied from 93–124.5, one-dimensional modeling is a proper choice for this design.

3.9. Optimization of Thermal Coupling Reactor for the Production of MEK. In this section, the genetic algorithm is used as a powerful tool to optimize the thermal coupling reactor. A genetic algorithm is a random search algorithm inspired by the nature [31, 32]. A GA tries to discover the most appropriate solution to a problem. The GA technique has repeated the natural survival for the best generation to form feature subsets (chromosomes) with the best performance in producing new feature chromosomes. As the population progresses from one generation to another, inappropriate solutions disappear, and appropriate ones are used. Each individual creates a chromosome in this method, and its colony is called a population. The fit function is applied to provide new solutions and used as operators such as duplication and mutation. To improve the optimized global network parameters, the GA uses three basic operators: selection, crossover, and mutation. Selection compares chromosomes in the population and chooses them to take part in the reproduction process. Selection also occurs with a given probability on the basis of the fitness function. Moreover, the recombination or crossover is carried out after finishing the selection process. It combines with predefined probability, features of two selected parent chromosomes, and forms similar children. Mutation characteristic is applied to create alternate subsets for each chromosome [32, 33]. Generally, mutation refers to the creation of a new chromosome from one and only one individual with predefined probability.

In this GA diagram, individuals are selected for intersection according to the fit function. After the crossover process, a predetermined rate for the jump is performed to avoid the local minimum. Adaptation values are calculated from the newly created generation at once. Old and inappropriate people replace new people to ensure that the population remains in a certain number until this reaches a certain number of generations; this process continues in the GA. After getting the mandatory termination value, the desired chromosome is considered in the solution [32]. This method can be very effective if the parameters are selected correctly. Figure 4 shows the process of solution using the genetic algorithm. As mentioned above, for optimization with a genetic algorithm, 3 main parameters in the problem must be determined by the user: the number of the initial population, mutations, and generation production which were, respectively, 40, 60, and 40%, in this research. In this paper, the sum of Fischer–Tropsch process products, output hydrogen, and their efficiency was considered as objective functions. The objective function can be defined as follows:

$$OF = \sum_{i=1}^{9} \frac{\text{products}_i}{F_1} + \sum_{j=1}^{2} \frac{\text{products}_j}{F_2} + \sum_{i=1}^{9} \text{yields} + \sum_{j=1}^{2} \text{yields}. \tag{33}$$

i and j show the number of components in the exothermic and endothermic parts, respectively.

Eight operational variables of the decision making for the optimization problem are:

(1) Input temperature of the exothermic part ($T_{0,\ \mathrm{Exo}}$)
(2) 2-molar flow rate of the exothermic part (($\mathrm{F}_{0,\ \mathrm{Exo}}$)
(3) Input temperature of the endothermic part ($T_{0,\ \mathrm{Endo}}$)
(4) Input molar flow rate of the endothermic part ($\mathrm{F}_{0,\ \mathrm{Endo}}$)
(5) Reactor length (L)
(6) Number of reactor tubes (n)
(7) The volume of the catalyst in the endothermic part of the reactor (V)
(8) The input pressure of the endothermic part of the reactor (P)

The range of these decision-making variables will be determined after sensitivity analyses. The following condition is applied to ensure that the CO conversion rate is higher than the ordinary reactors.

$$\text{Conversion} \geq 60\%. \tag{34}$$

The general form of the target function is presented below. The problem is thus optimized using a genetic algorithm.

$$OF = -F + 10^{15} GG = \max\{0, (0.6 - \text{conversion})\}. \tag{35}$$

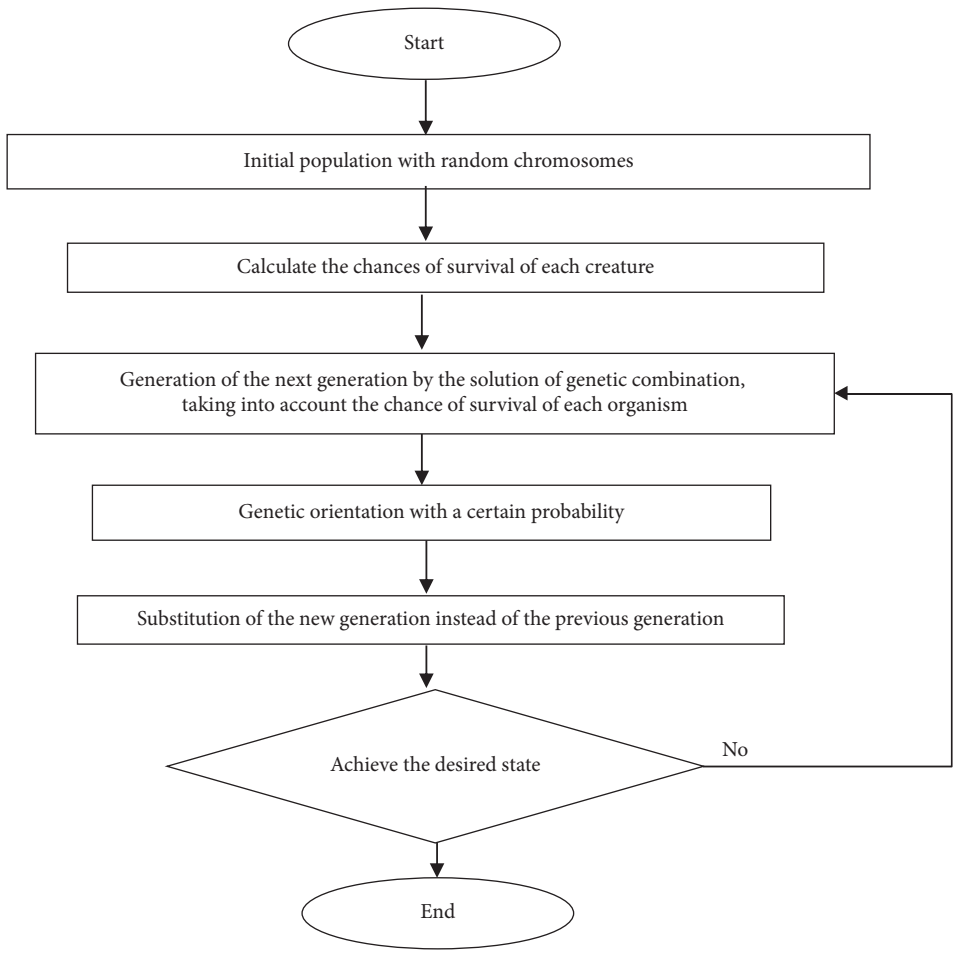

Figure 4: Solution steps in the genetic algorithm.

Table 2: Comparison of the experimental data with simulation results [36].

Parameters	Experimental data	Simulation results	Relative error
CO conversion	0.7794	0.754	3.25
H_2 conversion	0.9283	0.98	5.56
Output products (gmol/h)	19.96	18.74	6.1
Reactor output temperature (°C)	562	566	0.712

4. Evaluation of the Model

This section analyses the results of these equations in different modes, which include mass and energy balance equations, as well as their thermal coupling with an endothermic reaction and the optimization of the thermal coupling to produce products using the reaction heat. The governing equations are a set of ordinary differential equations including mass and energy equations. This set of equations must be coupled with the nonlinear algebraic equations of the kinetic, kinetics, and auxiliary equations. The finite-difference numerical method was applied to convert ordinary differential equations to nonlinear algebraic ones. To achieve this, the reactor length was divided into 100 separate sections and these equations were simultaneously solved for the reactor length by MATLAB software [34, 35]. The ReactorApp toolbox is structured as a set of MATLAB functions and classes, used by a graphical user interface (GUI) to receive the information and display the results. The MATLAB toolbox for dealing with chemical reactor engineering problems is as follows:

Simulation of ideal reactors (PFR, CSTR, and Batch reactors) even with bypass or recycling side streams

Simulating the connection of these reactors in series or parallel

Optimizing the design of reactors

Conversion versus temperature diagrams for reversible exothermic reactions.

4.1. Validation of the Model. The model was validated by comparing the simulation results with experimental data for the typical steady-state MEK production reactor with acceptable validity. The results are presented in Table 2.

4.2. Sensitivity Analysis. In this section, the influence of the operational conditions and design parameters in the aligned flow regime was assessed on the yield of MEK production and 2-butyl alcohol conversion.

Figure 5 assesses the changes in the conversion percentage of 2-butyl alcohol concerning the inlet temperature of the endothermic part. As the inlet temperature of the endothermic section decreased, the conversion percentage declined sharply. Although this temperature reduction is economically and operationally beneficial, the highest possible temperature should be adopted to avoid a low alcohol conversion rate.

Figure 6 depicts the changes in hydrogen conversion along the reactor length in terms of the exothermic part temperature. As seen, a decline in the temperature of this section from 650 to 500 K decreased the deriving force between these two sections (endothermic and exothermic) prohibiting the reaction onset in the exothermic (FT) part. Thus, the highest possible temperature should be selected in this section such that a rise in the driving force initiates the reaction in the exothermic part, elevating the temperature. This temperature elevation is in favor of production and can enhance hydrogen generation.

Figure 7 illustrates the variations in the conversion percentage *f* alcohol according to the molar flow rate on the exothermic part of the reactor. As expected, this volume of catalyst was not sufficient and declined the conversion due to the fixed amount of catalyst (200 mg) and flow rate increase. In this modeling, the molar flow rate was set at an optimal point of 1 mol/g to stabilize the conversion percentage at 30–35%.

Figure 8 shows the influence of molar flow rate on the exothermic part of the reactor on the conversion percentage of alcohol. As the heat generated in the exothermic part will be transported to the endothermic part, the variables should be set in such a way that the temperature on the exothermic side does not drop and decline the conversion percentage. As seen, a rise in the molar flow rate of the exothermic part (in constant catalyst volume) declined the conversion percentage, reducing the temperature or the produced heat, this will also decrement the heat traveling from the exothermic wall to the endothermic part. The alcohol conversion rate will also be decremented (endothermic part). Therefore, the input molar flow rate was considered as 0.236 mol/s which led to a conversion rate of 30% which is industrially acceptable.

Figure 9 illustrates the changes in CO conversion rate as a function of the molar flow rate of the endothermic part. The lower the molar flow rate in this section, the lower the cooling function. As the amount of heat in this section is enough, a rise in the molar flow rate from 0.5 to 2 mol/s caused no significant changes in the conversion rate. It can be said that the CO conversion rate had no significant dependence on the input molar flow rate of the endothermic part. Therefore, the molar flow rate of this section was set to 1 mol/s.

Figure 10 presents the variations in the CO conversion percentage as a function of the input molar flow rate of the exothermic part. As expected, a rise in the molar flow rate of the exothermic part, as well as an insufficient amount of catalyst, declined the conversion percentage. As the maximum CO conversion rate is 72% in industrial applications, in this modeling, the amount of 0.236 was chosen to provide both a high conversion rate and production yield.

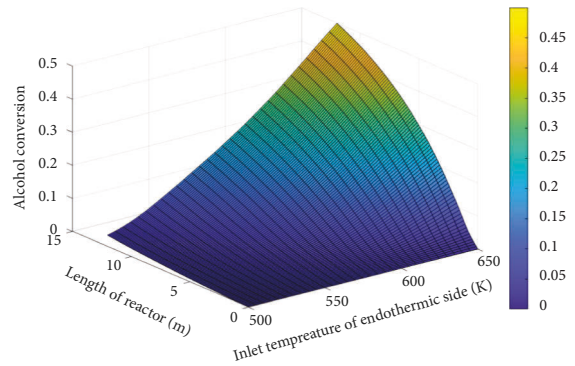

Figure 5: Effect of temperature on the endothermic side of the reactor on conversion percentage of 2-butyl alcohol and MEK yield.

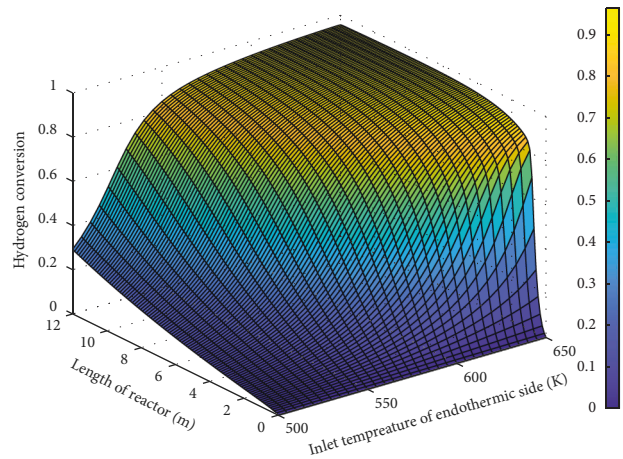

Figure 6: Effect of temperature on the exothermic side of the reactor on conversion percentage of 2-butyl alcohol and MEK yield.

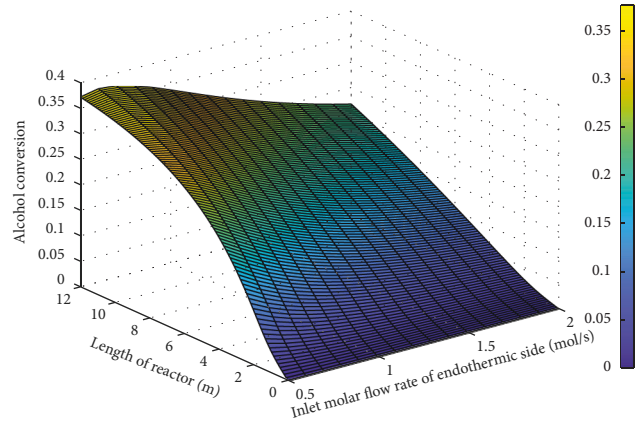

Figure 7: Effect of molar flow rate on the exothermic side of the reactor on conversion percentage of 2-butyl alcohol and MEK yield.

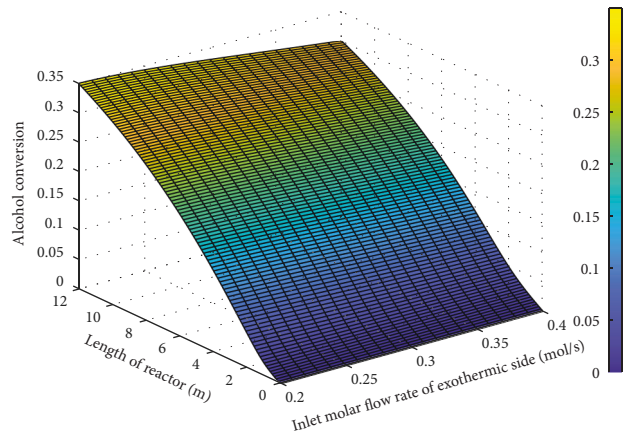

Figure 8: Effect of molar flow rate on the exothermic part of the reactor on conversion percentage of 2-butyl alcohol and MEK yield.

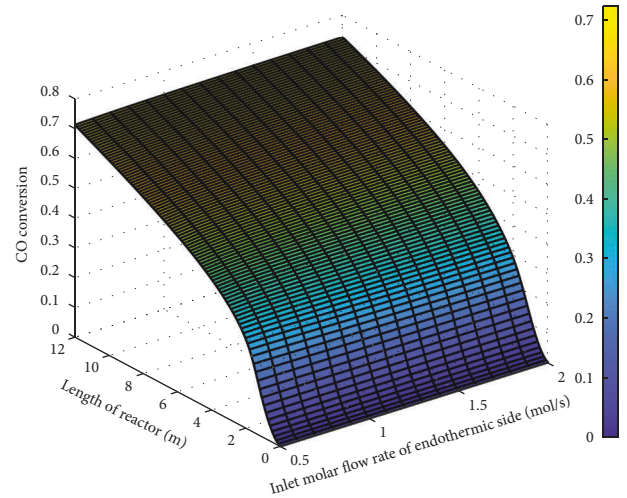

Figure 9: Effect of input molar flow rate at the endothermic part on conversion percentage of CO and MEK yield.

4.3. Optimization Parameters. In this section, the optimization range of the operational conditions is first selected. Then, using a genetic algorithm, these values will be obtained. The optimization range of the operational conditions were selected as follows:

$$\begin{aligned} 6L18\,(m),\\ 1n20,\\ 0.201F_1 0.335\left(\frac{\text{mol}}{s}\right),\\ 520T_1 610\,(K),\\ 0.2F_2 1.9\left(\frac{\text{mol}}{s}\right),\\ 580T_2 720\,(K). \end{aligned} \tag{36}$$

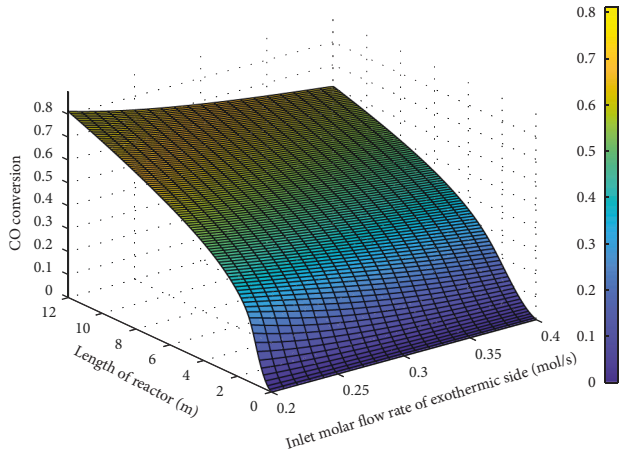

Figure 10: Effect of molar flow rate in the exothermic part on the CO conversion rate and MEK yield.

In the above equations, subscripts 1 and 2 denote exothermic and endothermic parts, respectively. Table 3 lists the optimal values of the parameters after optimization with a genetic algorithm.

4.4. Aligned Flow Regime Results for Three Modes of CFTR, TCFTR, and OTCFTR. In this section, the results are separately discussed for aligned flow in three modes of conventional FT reaction (CFTR), thermally coupled FT reaction (TCFTR), and optimized thermally coupled FT reaction (OTCFTR).

4.4.1. Variations in the Molar Flow Rate of the Materials along the Reactor Length. Figures 11–15 compare the molar behavior of various materials in the exothermic part of the reactor in three modes of CFR, TCFTR, and OTCFTR. Regarding the temperature sensitivity of the reaction, the production rate of the reactor rose by the temperature elevation. Despite some differences in the molar profile of various materials, this difference is due to better temperature control of TCFT and OTCFTR modes, the better results, were, however, obtained at the end of the reactor.

In recent years, hydrogen has been considered a clean fuel due to global warming as well as rising fossil fuel prices. As shown in Figure 10, a considerable amount of hydrogen was produced by this process (above 5 mol/s) which can be used as a clean fuel. In general, after coupling and optimization, the amount of hydrogen was increased by 0.022 mol/s. In the OTCFR mode compared to the TCFR mode, the molar flow rate as the feed of the exothermic part was increased by 0.014 mol/s.

Carbon dioxide is a toxic gas. It is, however, an important precursor in FT reaction for being converted into heavier organic products. According to Figure 11, the same explanation for the decline in the input molar flow rate at the exothermic part for hydrogen holds for the CO.

The exothermic part is associated with the dehydrogenation reaction in which hydrogen is one of the main products. A comparison of the hydrogen production of the

Table 3: Genetic algorithm optimization parameters.

Parameter	TCFTR	OTCFTR
Reactor length	12	11.86
Number of the reactor tube	1	5
Input temperature of the exothermic part of the reactor	569	569.45
Input molar flow rate of the exothermic part of the reactor	0.268	0.3614
Input molar flow rate of the endothermic part of the reactor	620	625.84
Input molar flow rate of the exothermic part of the reactor	1	1.1514

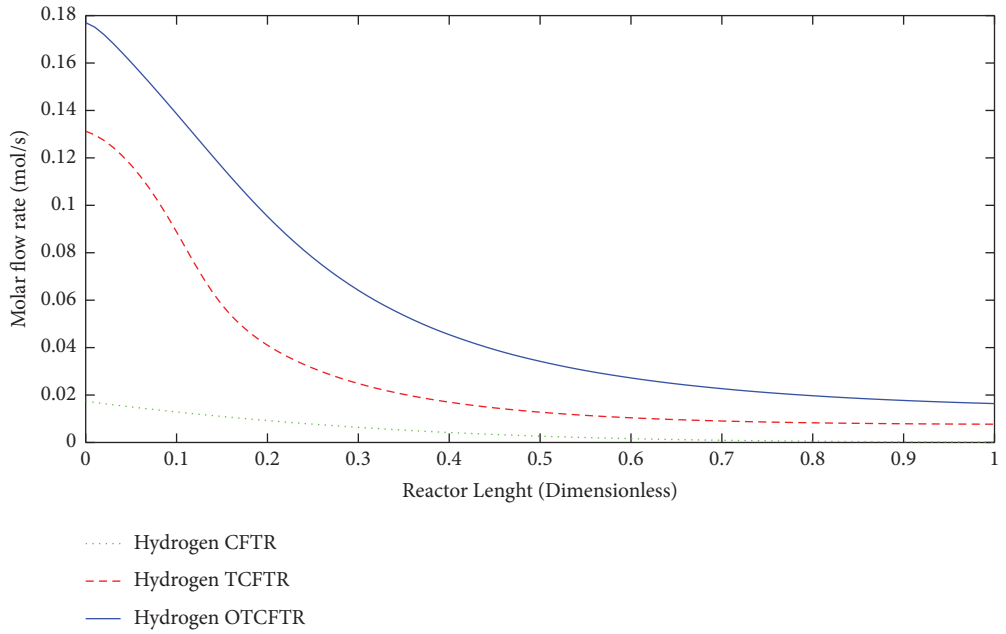

Figure 11: Hydrogen molar flow rate along the reactor length in CFTR, TCFTR, and OTCFTR.

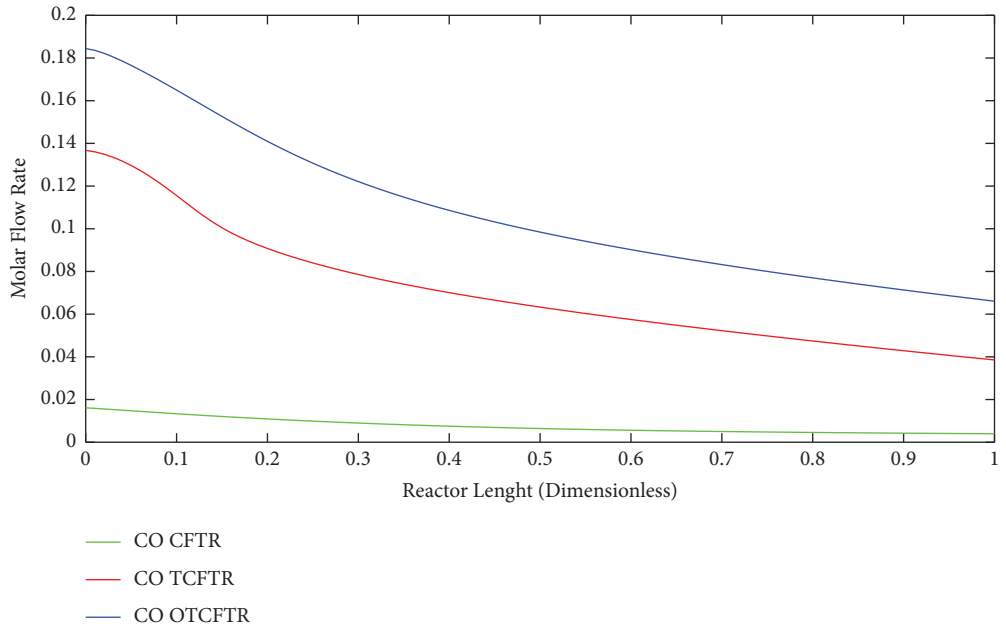

Figure 12: CO molar flow rate along the reactor length in CFTR, TCFTR, and OTCFTR modes.

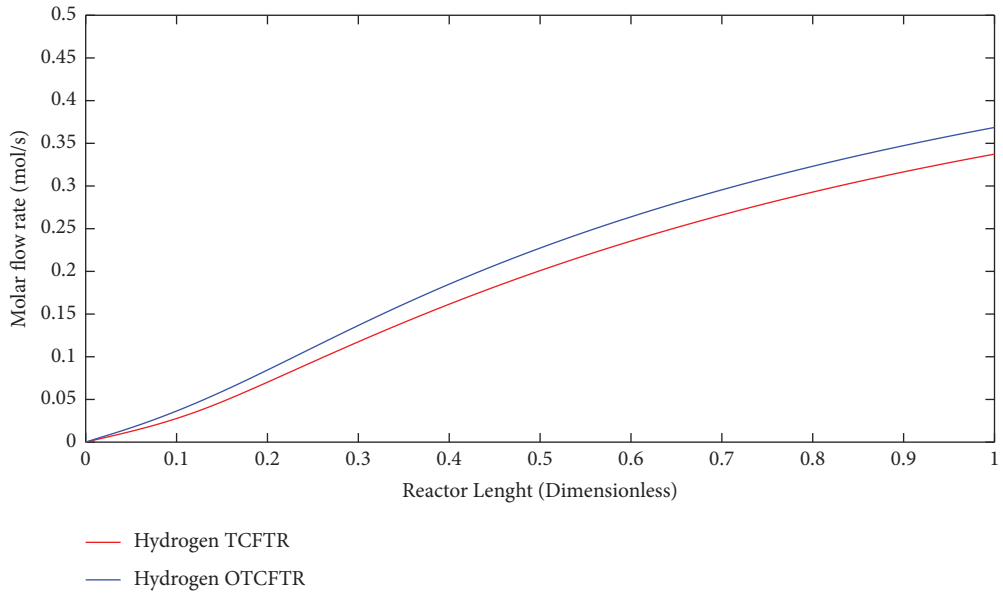

Figure 13: Comparison of the molar flow rate at the exothermic part for TCFTR and OTCFTR.

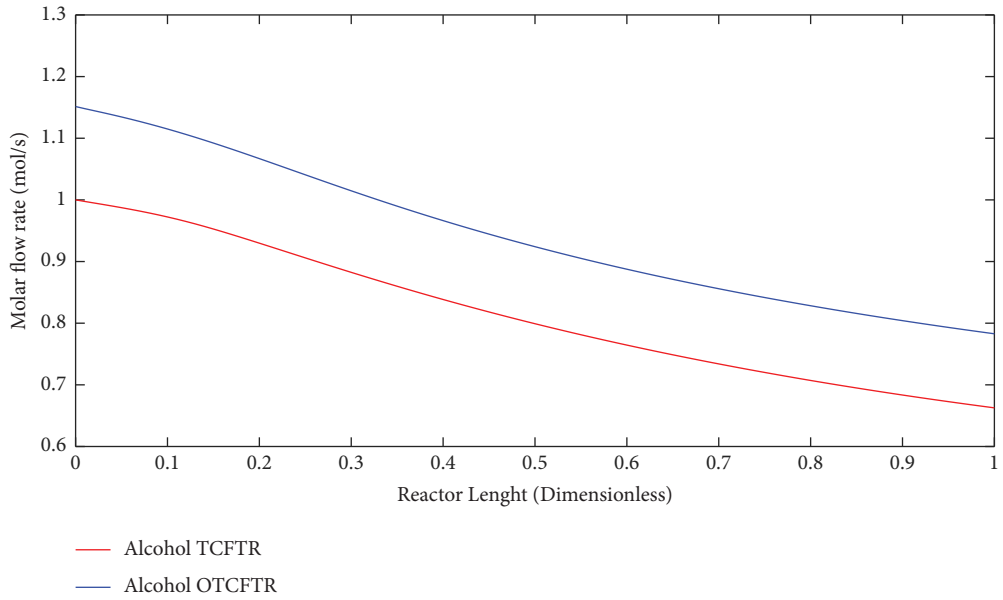

Figure 14: Comparison of the molar flow rate of 2-butyl alcohol in the exothermic part along the reactor length for TCFTR and OTCFTR.

coupled and optimized coupled process indicated a rise in hydrogen production after optimization.

2-butyl alcohol is highly used in various industries. Dehydrogenation of this material and production of MEK were studied in this paper. Using fewer amounts of this material at a lower price, the same conversion percentage was achieved for dehydrogenation products which are of crucial significance.

Methyl ethyl ketone is one of the most important and widely used chemicals that is used as a solvent in various industries. This article tried to achieve a cost-effective way by optimizing the production of this material. This diagram shows a rise in the production of this valuable substance after coupling as well as the optimization. Noteworthy, the conversion percentage of methyl ethyl ketone was enhanced to 35% by optimizing the temperature and consuming less energy to perform this exothermic reaction. Figures 16–22 show the changes in molar flow rates of the products of the exothermic reaction (Fischer–Tropsch products).

As seen, this material was produced in little amounts before the coupling process. After coupling and optimization, its amount exhibited a considerable increase. It is noteworthy that this increase in production was achieved with less raw material and energy use.

Ethane is a colorless hydrocarbon and one of the derivatives of natural gas. The refinery of this gas will result in

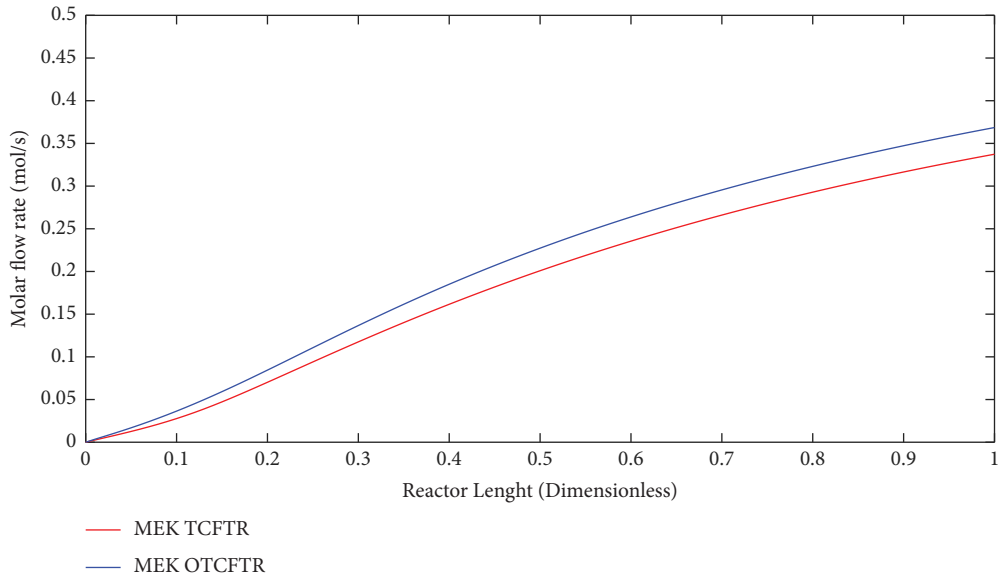

Figure 15: Comparison of the molar flow rate of MEK in the endothermic part of the reactor for TCFTR and OTCFTR.

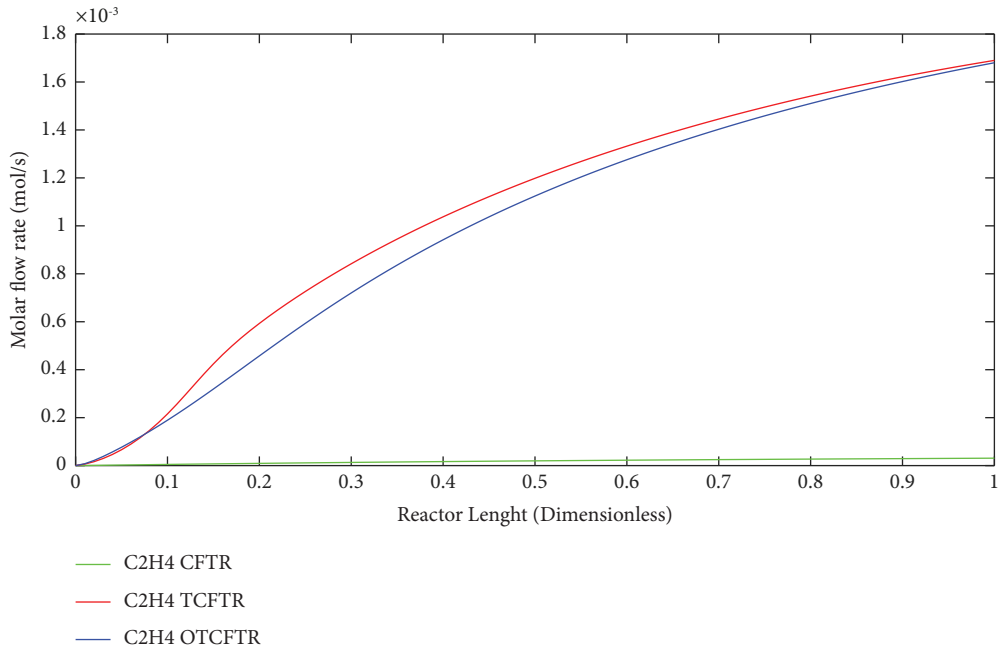

Figure 16: Comparison of the molar flow rate of ethylene in the exothermic part of the reaction for CFTR, TCFTR, and OTCFTR.

ethylene. Ethylene can be used as a fuel after compounding with methane. Ethane is also one of the products of FT reaction. As seen, the production of this material was drastically increased after coupling and optimization as well as temperature regulation.

Propane is a three-carbon alkane and is generally a colorless and odorless gas. It is often compressively liquified for the ease of transportation. This gas is one of the products of oil wells. It can also be produced in this reaction. As seen, MEK production was raised after coupling this exothermic reaction with the endothermic reaction of MEK production. Optimization of this process also considerably enhanced the production of this material.

The above figure shows the changes in the CO during FT reaction after coupling and optimization. The production of this material showed an apparent increase during these processes.

As suggested by the three above figures, the production of all three mentioned materials increased by coupling and optimization. The above figures, respectively, illustrate the changes in the production of gasoline, isobutene, and normal butane.

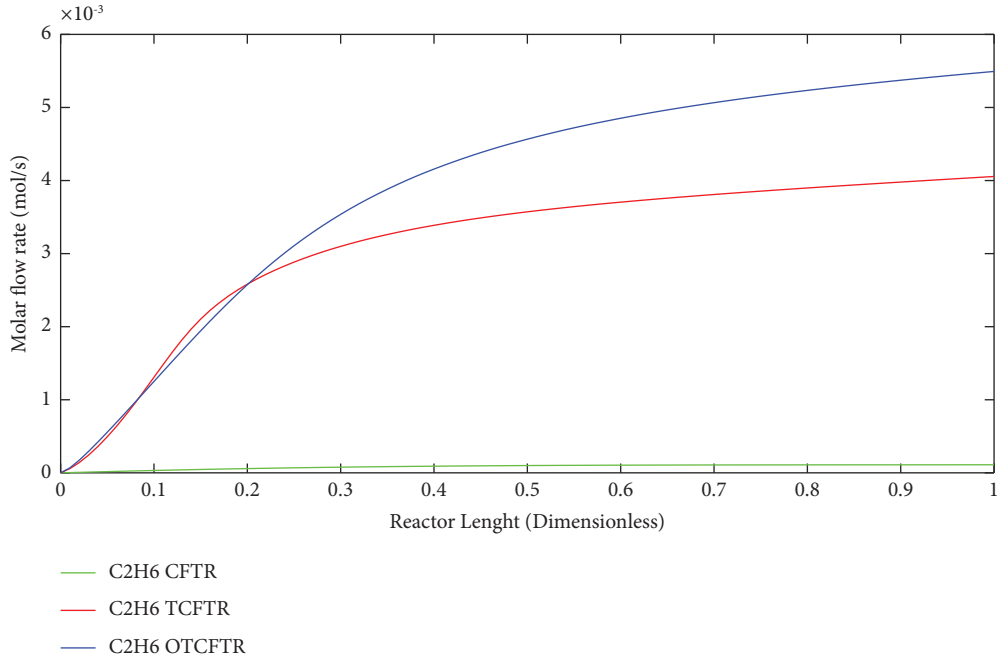

Figure 17: Comparison of the molar flow rate of ethane in the exothermic part of the reactor for CFTR, TCFTR, and OTCFTR.

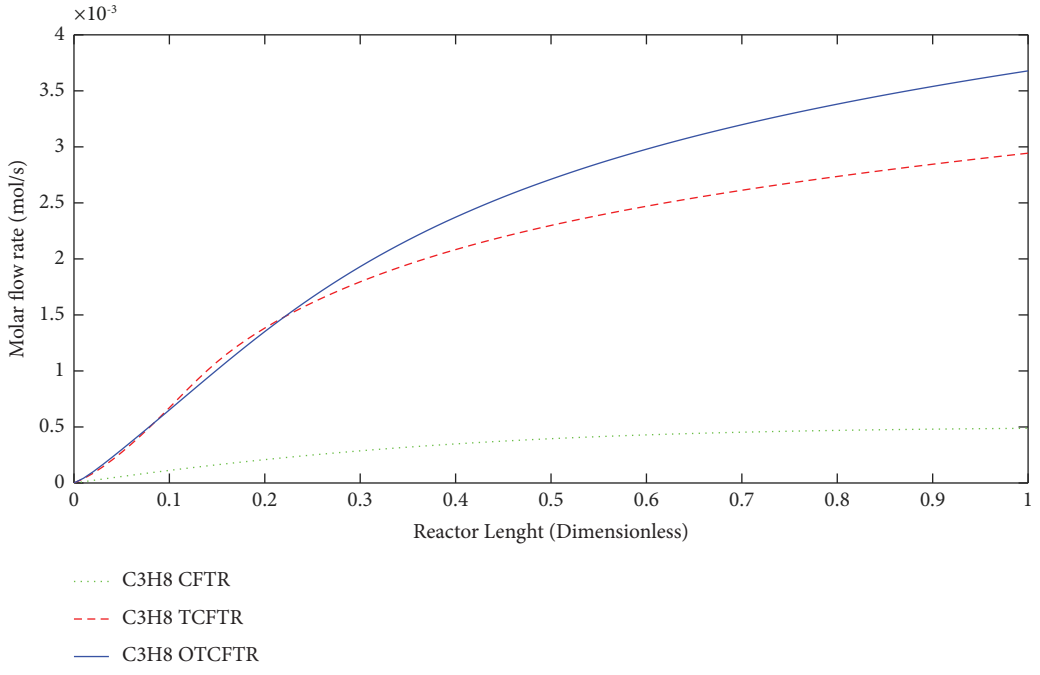

Figure 18: Comparison of the molar flow rate of propane in the exothermic part of the reactor for CFTR, TCFTR, and OTCFTR modes.

4.4.2. Temperature Profile along the Reactor Length. Figure 23 compares the temperature profile of the reactor in the endotherm section in TCFTR and OTCFTR modes. Regarding the endothermic nature of the reaction, there is a temperature increase at the beginning of the reactor. By consumption of raw materials, heat exchange, and the amount of heat transferred by the exothermic reaction, the temperature profile showed a linear drop, followed by an increment in the number of products. The heat sink increases. In both OTCFTR and TCFTR modes, the temperature declined at the end of the reactor to reach an equilibrium temperature. Heat is also transferred from the exothermic side resulting in a lower percentage of hydrogen conversion (Figure24).

Figure 25 compares the temperature profiles of the exothermic part of the reactor for different modes. Normally,

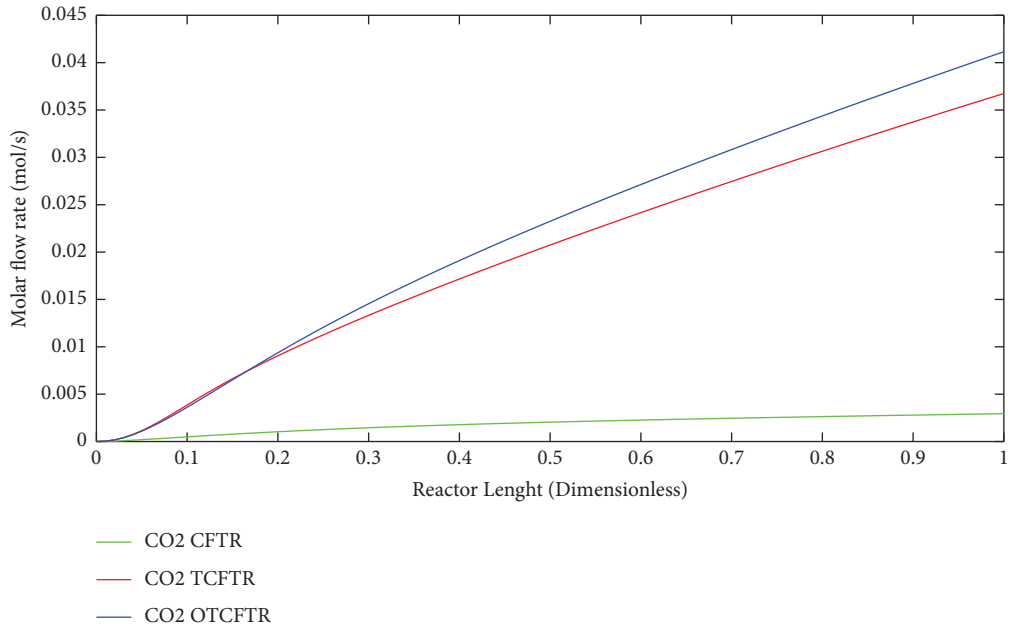

Figure 19: Comparison of the molar flow rate of CO in the exothermic part of the reactor for CFTR, TCFTR, and OTCFTR modes.

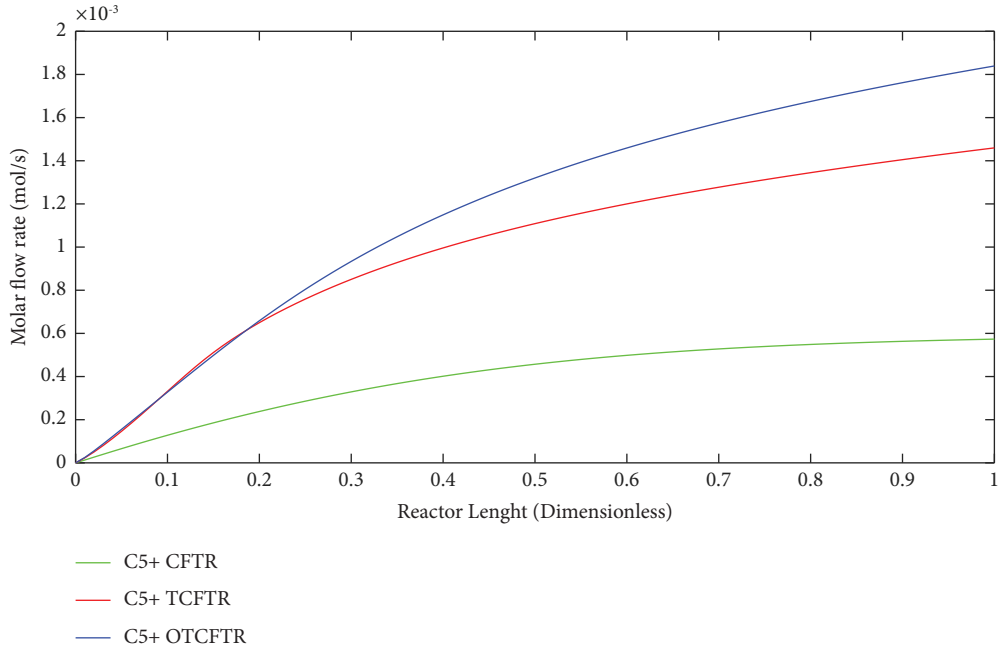

Figure 20: Comparison of the molar flow rate of gasoline in the exothermic part of the reactor for CFTR, TCFTR, and OTCFTR modes.

a constant temperature coolant is used to cool the reactor, which also imposes some costs on the process. In this paper, cooling costs were fully removed by an endothermic reaction, and better temperature control was achieved in the reactor. Also, the temperature profile in the reactor significantly decreased along the reactor length. Another advantage of better control of the reactor temperature is the delayed deactivation of the catalysts. OTCFTR mode increased the MEK production and the conversion percentage of 2-butyl alcohol due to the optimization. A slight increase was observed in output temperature compared to the TCFTR mode, which is acceptable.

4.4.3. Analysis of Conversion Percentage of Raw Materials along the Reactor Length. In this section, the conversion percentage of hydrogen and carbon monoxide is analyzed along the reactor length in different modes (Figures 24 and

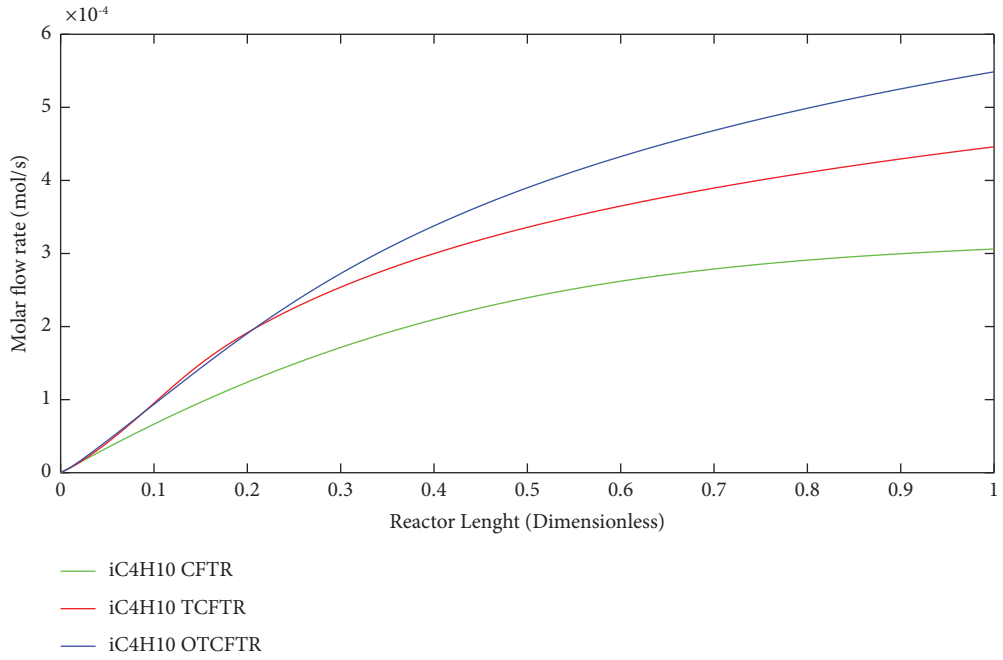

Figure 21: Comparison of the molar flow rate of isobutene in the exothermic part of the reactor for CFTR, TCFTR, and TCFTR modes.

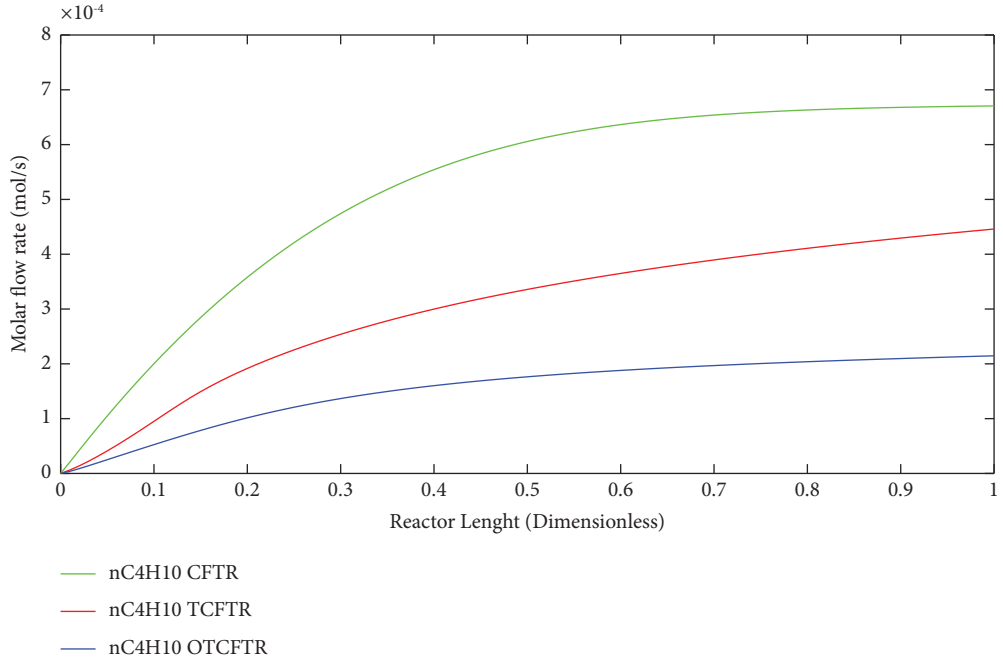

Figure 22: Comparison of the molar flow rate of normal butane in the exothermic part of the reactor for CFTR, TCFTR, and OTCFTR modes.

26). Compared to CFTR, TCFTR, and OTCFTR in addition to higher MEK production led to a decrease in the conversion percentage of hydrogen. By consuming lower amounts of raw materials (reactants), this method reduced the cost of raw material supply and consequently declined the separation costs of the process.

As can be seen, by consuming lower amounts of material due to the smaller conversion percentage of hydrogen, higher product yields were achieved.

In this paper, by minimizing and maximizing various parameters, it was tried to reduce operating costs, consumption of raw materials, and separation costs while

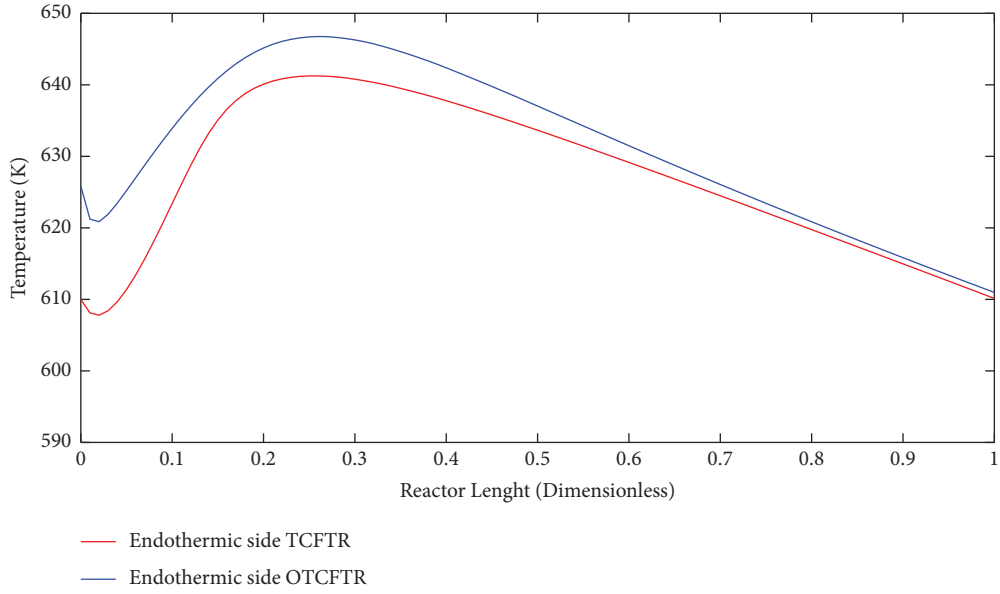

Figure 23: Comparison of the temperature profiles in TCFTR and OTCFTR modes in the endothermic part of the reactor.

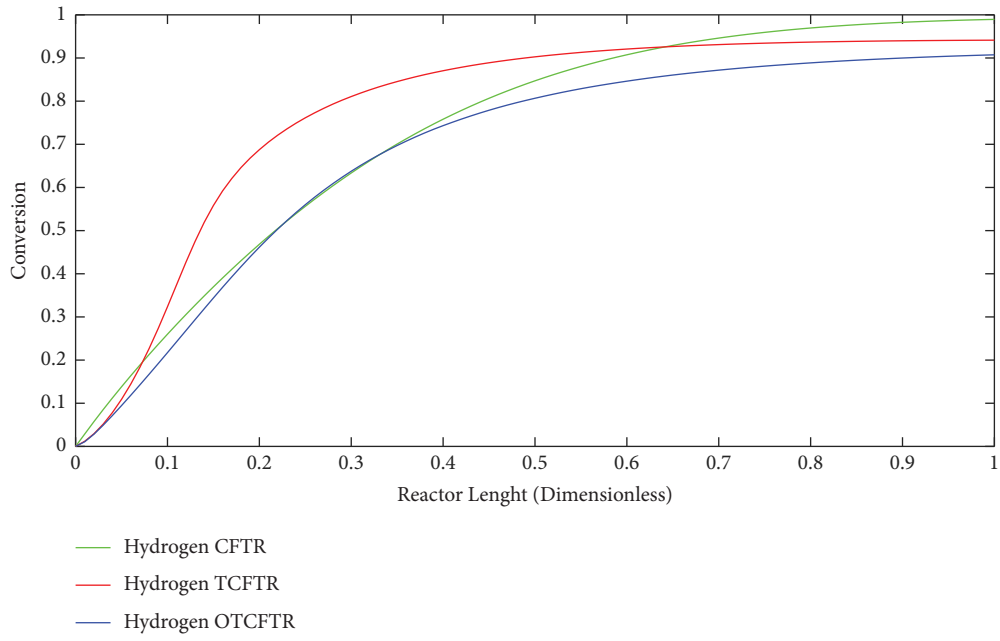

Figure 24: Conversion percentage of hydrogen in various modes along the reactor length.

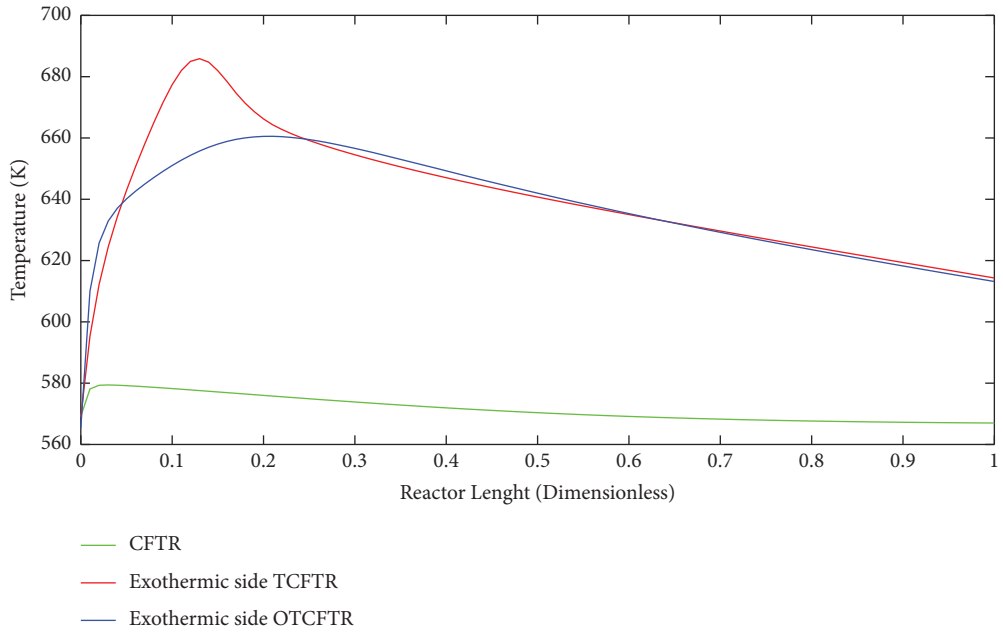

Figure 25: Comparison of temperature profiles in different states of the exothermic section along the reactor length.

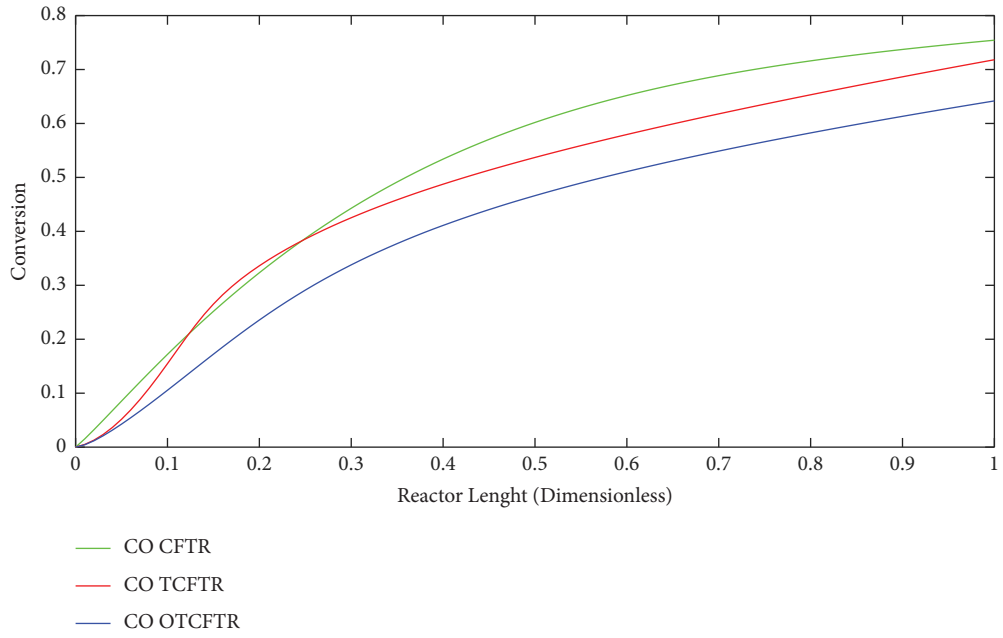

Figure 26: Conversion percentage of carbon monoxide in various modes along the reactor length.

enhancing the efficiency of MEK production; and improving this process in the industry.

5. Conclusion

In this work, we presented a novel multifunctional reactor to progress catalytic dehydrogenation reaction of 2-butanol and MEK production. Accordingly, the heat required for thermally coupled reactor and also dehydrogenation of 2-butanol is supplied by the FT reaction through gas to liquid (GTL) method as an exothermic reaction utilizing spherical ZnO catalyst. In this paper, by minimizing and maximizing various parameters, we propose techniques to reduce operating costs, consumption of raw materials, and separation costs while enhancing the efficiency of MEK production, and improving this process in the industry. We employed an evolutionary genetic algorithm to optimize the reactor for the operating conditions of the reaction while maintaining the efficiency and conversion percentage. MATLAB software was also utilized for modeling and optimization. It is worthy

to note that the results are separately discussed for aligned flow in three modes of conventional FT reaction (CFTR), thermally coupled FT reaction (TCFTR), and optimized thermally coupled FT reaction (OTCFTR). We found out that after coupling and optimization, the amount of hydrogen increases by 0.022 mol/s. In the OTCFR mode compared to the TCFR mode, the molar flow rate as the feed of the exothermic part was increased by 0.014 mol/s. Notably, the modeling results were verified by industrial data and also indicated a 37% and 55.4% increase in the production rate of thermal coupling and optimal thermal coupling reactors, respectively.

Data Availability

Data sharing is not applicable for this manuscript because the results of this research are related to a private company.

Conflicts of Interest

The authors declare that they have no conflicts of interest.

References

[1] D. Iranshahi, "Mathematical modeling of a multi-stage naphtha reforming process using novel thermally coupled recuperative reactors to enhance aromatic production," *International Journal of Hydrogen Energy*, vol. 35, pp. 10984–10993, 2010.

[2] F. Samimi, S. Kabiri, and M. R. Rahimpour, "The optimal operating conditions of a thermally double coupled, dual membrane reactor for simultaneous methanol synthesis, methanol dehydration and methyl cyclohexane dehydrogenation," *Journal of Natural Gas Science and Engineering*, vol. 19, pp. 175–189, 2014.

[3] P. Compton, N. R. Dehkordi, M. Knapp, L. A. Fernandez, A. N. Alshawabkeh, and P. Larese-Casanova, "Heterogeneous fenton-like catalysis of electrogenerated H2O2 for dissolved RDX removal," *Frontiers in Chemical Engineering*, vol. 47, 2022.

[4] R. Ghani and D. Iranshahi, "Conceptual comparison of four configurations in the thermal coupling of ammonia synthesis and 2-butanol dehydrogenation," *Applied Thermal Engineering*, vol. 154, pp. 238–250, 2019.

[5] A. H. Alibak, M. Khodarahmi, P. Fayyazsanavi, S. M. Alizadeh, A. J. Hadi, and E. Aminzadehsarikhanbeglou, "Simulation the adsorption capacity of polyvinyl alcohol/carboxymethyl cellulose based hydrogels towards methylene blue in aqueous solutions using cascade correlation neural network (CCNN) technique," *Journal of Cleaner Production*, vol. 19, 2022.

[6] O. Jahanmahin, D. J. Kirby, B. D. Smith et al., "Assembly of gold nanowires on gold nanostripe arrays: simulation and experiment," *Journal of Physical Chemistry C*, vol. 124, no. 17, pp. 9559–9571, 2020.

[7] G. Bai, "Influence of acid–base properties of the support on copper-based catalysts for catalytic dehydrogenation of 2-butanol," *Catalysis Letters*, vol. 143, pp. 101–107, 2013.

[8] J. J. Perona and T.. George, "Reaction kinetic studies: catalytic dehydrogenation of sec-butyl alcohol to methyl ethyl ketone," *AIChE Journal*, vol. 2, pp. 230–235, 1957.

[9] M. Shakeri, D. Iranshahi, and A. Naderifar, "Optimization of a novel multifunctional reactor containing m-xylene hydrodealkylation and naphtha reforming," *International Journal of Hydrogen Energy*, vol. 44, pp. 21882–21895, 2019.

[10] M. Fatholahi, A. Anvari, O. A. Akbari et al., "Numerical investigation of mixed convection of nanofluid flow in oblique rectangular microchannels with nanofluid jet injection," *The European Physical Journal Plus*, vol. 136, no. 10, p. 1062, 2021.

[11] S. Ebrahimian and D. Iranshahi, "A conceptual comparison between potential configurations in the thermal coupling of naphtha reforming with propane ammoxidation," *International Communications in Heat and Mass Transfer*, vol. 112, 2020.

[12] J. N. Keuler and L.. Leon, "The dehydrogenation of 2-butanol in a Pd–Ag membrane reactor," *Journal of Membrane Science*, vol. 202, pp. 17–26, 2002.

[13] A. Nemati Kharat, F. Rajabi Kouchi, and B. Tamaddoni Jahromi, "Markovnikov hydroformylation catalyzed by ROPAC in the presence of phosphine and phosphine oxide ligands," *Journal of Coordination Chemistry*, vol. 69, no. 1, pp. 12–19, 2016.

[14] N. R. Dehkordi, M. Knapp, P. Compton, L. A. Fernandez, A. N. Alshawabkeh, and P. Larese-Casanova, "Degradation of dissolved RDX, NQ, and DNAN by cathodic processes in an electrochemical flow-through reactor," *Journal of Environmental Chemical Engineering*, vol. 10, no. 3, 2022.

[15] https://link.springer.com/article/10.1007/s11042-020-10139-6.

[16] M. A. Marvast, "Fischer-tropsch synthesis: modeling and performance study for Fe-HZSM5 bifunctional catalyst," *Chemical Engineering and Technology*, vol. 28, pp. 78–86, 2005.

[17] N. Ebrahimi, S. Adelian, S. Shakerian et al., "Crosstalk between ferroptosis and the epithelial-mesenchymal transition: implications for inflammation and cancer therapy," 2022, https://www.sciencedirect.com/science/article/pii/S1359610122000065.

[18] G. B. W. L. Ligthart, "Highly sustainable catalytic dehydrogenation of alcohols with evolution of hydrogen gas," *Tetrahedron Letters*, vol. 44, pp. 1507–1509, 2003.

[19] L. I. U. Zhenhua, "Development and commercial application of methyl-ethyl-ketone production technology," *Chinese Journal of Chemical Engineering*, vol. 14, pp. 676–684, 2006.

[20] F. Faress, A. Yari, F. Rajabi Kouchi et al., "Developing an accurate empirical correlation for predicting anti-cancer drugs' dissolution in supercritical carbon dioxide," *Scientific Reports*, vol. 12, no. 1, pp. 1–17, 2022.

[21] D. Fang, "Synthesis and applications of mesoporous Cu-Zn-Al2O3 catalyst for dehydrogenation of 2-butanol," *Journal of Natural Gas Chemistry*, vol. 18, pp. 179–182, 2009.

[22] G. Chabot, "A mathematical modeling of catalytic milli-fixed bed reactor for Fischer–Tropsch synthesis: influence of tube diameter on Fischer Tropsch selectivity and thermal behavior," *Chemical Engineering Science*, vol. 127, pp. 72–83, 2015.

[23] A. Multer, "Production of methyl ethyl ketone from biomass using a hybrid biochemical/catalytic approach," *Industrial & Engineering Chemistry Research*, vol. 52, pp. 56–60, 2012.

[24] H. Torabi, M. Hoseini, M. Sadrkhah, G. Faraji, and A. Masoumi, "Microstructure, mechanical properties and biocorrosion properties of Mg-HA bionanocomposites fabricated by a novel severe plastic deformation process," *Ceramics International*, vol. 46, no. 3, pp. 2836–2844, 2020.

[25] G. D. DiVincenzo, C. J. Kaplan, and J. Dedinas, "Characterization of the metabolites of methyl n-butyl ketone, methyl iso-butyl ketone, and methyl ethyl ketone in Guinea pig serum and their clearance," *Toxicology and Applied Pharmacology*, vol. 36, pp. 511–522, 1976.

[26] S. M. A. Hashemi, A. Pirmoradi, and E. Zabeh, "Chaos control in virtual cathode oscillator by cathode structural optimization," 2015, https://www.researchgate.net/publication/344948332_Chaos_Control_in_Virtual_Cathode_Oscillator_by_Cathode_Structural_Optimization.

[27] O. Faraz, M. Poustchi, E. N. Denyani, P. Movahedi, F. R. Kouchi, and R. Shahriari, "Thermodynamic modeling of pharmaceuticals solubility in pure, mixed and supercritical solvents," *Journal of Molecular Liquids*, vol. 353, 2022.

[28] M. Trik, S. Pour Mozaffari, and A. M. Bidgoli, "Providing an adaptive routing along with a hybrid selection strategy to increase efficiency in noc-based neuromorphic systems," 2021, https://pubmed.ncbi.nlm.nih.gov/34567105/.

[29] A. Miyamoto and Y. Ogino, "Studies on catalysis by molten metal. V. Kinetics of the dehydrogenation of sec-butyl alcohol over the liquid indium catalyst," *Journal of Catalysis*, vol. 27, pp. 311–321, 1972.

[30] https://www.accessengineeringlibrary.com/content/book/9780071422949.

[31] W. W. Bailey, E. P. Maglaughlin, and W. H. Nichols, "Recovery of ethanol from a methyl ethyl ketone-ethyl acetate fraction such as produced by hydrocarbon oxidation," *U.S. Patent*, vol. 3, 1968.

[32] S. Mokhtari, K. D. Skelly, E. A. Krull et al., "Copper-containing glass polyalkenoate cements based on SiO 2–ZnO–CaO–SrO–P 2 O 5 glasses: glass characterization, physical and antibacterial properties," *Journal of Materials Science*, vol. 52, no. 15, pp. 8886–8903, 2017.

[33] https://academic.oup.com/jamia/article/27/7/1007/5848291.

[34] M. Trik, A. M. N. G. Molk, F. Ghasemi, and P. Pouryeganeh, "A hybrid selection strategy based on traffic analysis for improving performance in networks on chip," *Journal of Sensors*, vol. 2022, Article ID 3112170, 19 pages, 2022.

[35] https://de.mathworks.com/matlabcentral/fileexchange/76917-reactorapp-toolbox.

[36] J. A. Velasco, "Synthesis gas production for GTL applications: thermodynamic equilibrium approach and potential for carbon formation in a catalytic partial oxidation pre-reformer," *Journal of Natural Gas Science and Engineering*, vol. 20, pp. 175–183, 2014.

[37] R. Ghani and D. Iranshahi, "Comparison of co-current and counter-current flow in a bifunctional reactor containing ammonia synthesis and 2-butanol dehydrogenation to MEK," *International Journal of Hydrogen Energy*, vol. 44, pp. 2905–2917, 2019.